Facilitated transport and diffusion take distinct spatial routes through the nuclear pore complex

Jindriska Fiserova[1], Shane A. Richards[1], Susan R. Wente[2] and Martin W. Goldberg[1,*]

[1]Department of Biological and Biomedical Sciences, Durham University, South Road, Durham, DH1 3LE, UK
[2]Department of Cell and Developmental Biology, Vanderbilt University School of Medicine, U-3209 MRBIII, Nashville, TN 37232, USA
*Author for correspondence (m.w.goldberg@durham.ac.uk)

Accepted 5 May 2010
Journal of Cell Science 123, 2773-2780

doi:10.1242/jcs.070730

Summary

Transport across the nuclear envelope is regulated by nuclear pore complexes (NPCs). Much is understood about the factors that shuttle and control the movement of cargos through the NPC, but less has been resolved about the translocation process itself. Various models predict how cargos move through the channel; however, direct observation of the process is missing. Therefore, we have developed methods to accurately determine cargo positions within the NPC. Cargos were instantly trapped in transit by high-pressure freezing, optimally preserved by low-temperature fixation and then localized by immunoelectron microscopy. A statistical modelling approach was used to identify cargo distribution. We found import cargos localized surprisingly close to the edge of the channel, whereas mRNA export factors were at the very centre of the NPC. On the other hand, diffusion of GFP was randomly distributed. Thus, we suggest that spatially distinguished pathways exist within the NPC. Deletion of specific FG domains of particular NPC proteins resulted in collapse of the peripheral localization and transport defects specific to a certain karyopherin pathway. This further confirms that constraints on the route of travel are biochemical rather than structural and that the peripheral route of travel is essential for facilitated import.

Key words: Nucleocytoplasmic transport, Nuclear pore complex, mRNA export, Protein import, Transmission electron microscopy

Introduction

Nuclear pore complexes (NPCs) are the sole gates for regulated exchange of macromolecules between the nucleus and the cytoplasm. NPCs are composed of a cylindrical channel spanning the two membranes of the nuclear envelope (NE) and have opposing peripheral structures – the nuclear basket and cytoplasmic filaments (Goldberg and Allen, 1996; Yang et al., 1998; Stoffler et al., 2003) (for a review, see Lim et al., 2008). Controversy remains over the organization of the central channel, knowledge of which is crucial for understanding the processes that govern exchange between the nucleus and the cytoplasm.

The first three-dimensional models that were developed to describe the structure of vertebrate and yeast NPCs proposed a centrally located transporter (Akey and Radermacher, 1993; Yang et al., 1998). More recently, the central channel has been suggested to contain a randomly organized network of unfolded phenylalanine-glycine (FG) domains (Patel et al., 2007). About one-third of the proteins composing the NPC (nucleoporins or Nups) contain FG domains, which constitute up to 10% of the NPC mass (Devos et al., 2006). These domains adopt no secondary structure (Bayliss et al., 2000), and are thought to be unfolded and highly dynamic (Denning et al., 2003; Lim et al., 2007).

The translocation of most cargos through the NE is facilitated by karyopherins (Kaps). After binding to the cargo, Kaps are capable of overcoming the diffusion barrier of the NPC by an unconfirmed mechanism. Various models have been developed to describe the nature of the diffusion barrier and the means of translocation through the NPC (Rout et al., 2000; Ben Efraim and Gerace, 2001; Macara, 2001; Ribbeck and Gorlich, 2001). Despite recent progress in this area (Peters, 2005; Lim et al., 2007; Frey and Gorlich, 2007), it is still not known where within the NPC diffusion of smaller molecules takes place, and whether the biochemical translocation routes of distinct cargos through the channel are spatially separated or overlapping.

The interaction between Kaps and FG Nups is crucial for translocation, and numerous biochemical Kap–FG-Nup interactions have been documented (Iovine et al., 1995; Iovine and Wente, 1997; Marelli et al., 1998; Solsbacher et al., 2000; Denning et al., 2001; Bayliss et al., 2002; Matsuura et al., 2003). Messenger ribonucleoprotein (mRNP) export is a complex coordinated process facilitated by nuclear transport factor Mex67 (known as TAP in humans) and many adaptor proteins (for a review, see Iglesias and Stutz, 2008). Mex67/TAP triggers mRNP targeting to the NPC and the first steps of mRNA translocation. The terminal stage of mRNP export is mediated by DEAD-box protein Dbp5, among other adaptor proteins. Upon activation with Gle1, Dbp5 promotes mRNP remodelling and release from the NPC (Tran et al., 2007; Bolger et al., 2008), and has a role in directionality and efficiency. Both Dbp5 and Gle1 have binding sites at the cytoplasmic NPC side, namely at Nup159 and Nup42, respectively (Hodge et al., 1999; Schmitt et al., 1999). Similarly to the Kap import process, Mex67/TAP interacts with a subset of Nup FG domains. Biochemical evidence suggested that Kap95 might use different FG-binding sites to Mex67/TAP (Strawn et al., 2001; Allen et al., 2002; Blevins et al., 2003); this was further confirmed in deletion mutant screens (Terry and Wente, 2007). However, whether mRNA export occupies a spatially different part of the NPC channel to protein import remains unclear.

Separation of active and passive transport was suggested by early three-dimensional models (Hinshaw et al., 1992; Akey and Radermacher, 1993; Yang et al., 1998). Other studies have shown that transport and passive diffusion do not compete with each other (Naim et al., 2007; Kramer et al., 2008). This suggests the functional or structural segregation of transport from passive diffusion.

Journal of Cell Science

However, contradictory observations of a common pathway for both passive and facilitated transport have also been reported (Feldherr and Akin, 1997; Keminer et al., 1999; Mohr et al., 2009). The requirement for specific FG domains for mRNA export was shown previously in an FG-domain deletion screen (Terry and Wente, 2007). The same study also confirmed the existence of functionally independent active translocation pathways for Kap121 or Kap104 cargo transport; however, the study neither identified the spatial relationship between the import and export translocation routes nor tested for high-resolution changes in the NPC structure relating to the deletions (Terry and Wente, 2007).

To address the spatial relationships between various translocation routes within the NPC, we further developed the work of Terry and Wente (Terry and Wente, 2007). Using an immunoelectron microscopy approach, we quantified the spatial organization of different transport routes through the NPC for protein import via either Kap104 or Kap121. We then compared this with the positions of mRNA export factors Gle1 and Dbp5, and investigated the affects of FG-domain deletions on these routes. Importantly, we also followed the passive diffusion of unconjugated GFP to confirm or reject the existence of common or separate pathways for active and passive passage. Our analysis demonstrates distinct routes through the NPC and alterations of the route due to deletion of specific FG domains. The data also clearly distinguished active translocation routes from the passive diffusion of free GFP. Our findings provide new information on the mechanisms of translocation though the NPC.

Results

Spatially separated transport routes through the NPC

In this work, we aimed to characterize the locations of import and export routes through the NPC in *Saccharomyces cerevisiae*. Currently, electron microscopy is the only way to look directly at both structural and functional features of the nucleocytoplasmic transport process. By developing methods involving high-pressure freezing of live yeast cells, followed by low-temperature fixation and embedding (Walther and Ziegler, 2002), we developed a strategy to reveal NPC details within whole cells, with coincident immunogold labelling of transport factors and cargos as markers of transport routes. Because cells are instantly frozen, molecules in transit are instantly trapped within the NPC channel. This is an important point because translocation is a rapid process and slow chemical fixation is unlikely to capture it. An inevitable consequence of this approach is that there is no direct control of where sections through NPCs are cut. Because of the cylindrical shape of the NPC channel, few sections will be cut through the NPC centre, whereas all sections run through the NPC edge. To account for this unavoidable bias, we developed a novel statistical modelling approach that allowed us to quantify the spatial distribution of labelled proteins within the NPC instantly trapped by cryofixation.

We collected data describing the positions of the proteins involved in transport within the NPC using transmission electron microscopy (TEM) in cryofixed and freeze-substituted yeast. To follow the protein import routes, we immunogold labelled sections of wild-type yeast transformed with Nab2-NLS-GFP [a marker of Kap104 import (Chaves and Blobel, 2001; Strawn et al., 2004)] and Spo12-NLS-GFP [a marker of Kap121 import (Shulga et al., 2000; Strawn et al., 2004)] with an anti-GFP antibody. To indicate the route of mRNA export, we stained sections with antibodies against the mRNA export factors Gle1 [anti-Gle1 (Suntharalingam et al., 2004)] and Dbp5 (Bolger et al., 2008), which function in the remodelling of the mRNP as it exits the NPC (Alcazar-Roman et al., 2006; Weirich et al., 2006; Tran et al., 2007). Thus, labelling of Gle1 and Dbp5 provides markers for a terminal stage of mRNA export. Finally, we followed the diffusion of GFP through the NPC in yeast that expressed unconjugated GFP. The representative examples of electron micrographs displayed in Figs 1, 2 and 3 show that the various translocation marker proteins localized at different parts of the NPC channel. Kap104 and Kap121 cargos often localized near the NPC periphery (Fig. 1), whereas the mRNA export factors Gle1 and Dbp5 were predominantly located at the NPC centre (Fig. 2). Interestingly, GFP seemed to have no preference for any part of the NPC channel (Fig. 3).

To confirm this observation statistically, we sought the probability density functions (PDFs) that describe the likelihood of markers of import, export and diffusion being transported within the NPC relative to its central axis. First, we determined the exact

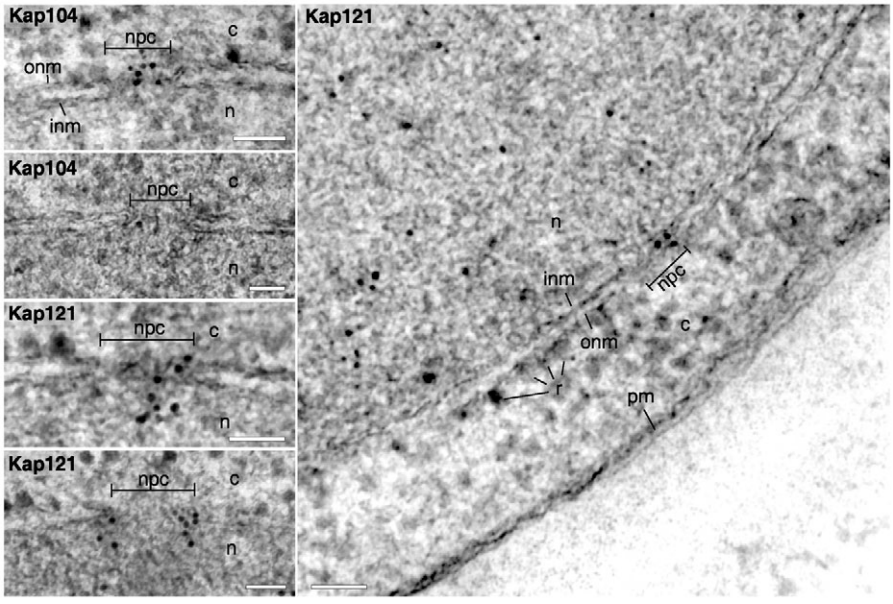

Fig. 1. Import of Kap121 and Kap104 cargo proteins as viewed on thin sections of high-pressure frozen, freeze-substituted and immunogold-labelled yeast. Representative TEM micrographs of yeast transformed with markers for Kap104 (Nab2-NLS-GFP) and Kap121 (Spo12-NLS-GFP) import immunolabelled with polyclonal anti-GFP primary antibody and anti-rabbit secondary antibody conjugated to 5 nm gold. Note the preferentially peripheral locations of the gold particles. n, nucleus; c, cytoplasm; npc, nuclear pore complex; inm, inner nuclear membrane; onm, outer nuclear membrane; r, ribosome; pm, plasma membrane. Scale bars: 50 nm.

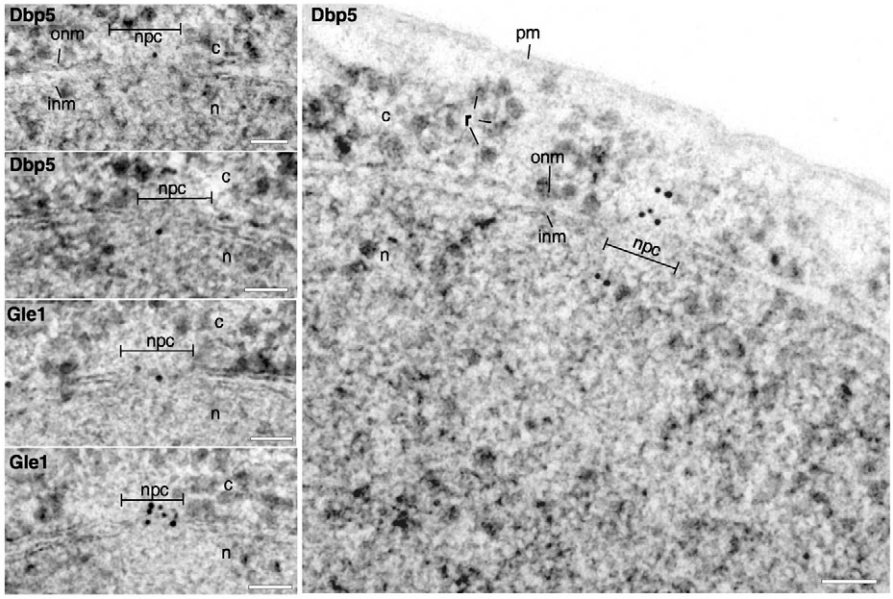

Fig. 2. Gle1 and Dbp5 located preferentially in the centre of the NPC. Representative TEM micrographs of high-pressure frozen and freeze-substituted wild-type yeast immunolabelled with polyclonal anti-Gle1 and anti-Dbp5 primary antibodies and anti-rabbit secondary antibody conjugated to 5 nm gold. Note the preferentially central locations of the gold particles. Scale bars: 50 nm.

location of the gold particle (reflecting the position of the translocation event) within the NPC central channel by measuring the width of the sectioned NPC (*l*) and the position of the gold particle in relation to the sectioned NPC central axis (*y*), assuming that the NPC diameter is constant. Fig. 4A illustrates the relationship between the section location within the NPC and the actual locations of the gold particles in relation to the NPC centre (for details, see Materials and Methods). Fig. 4B shows how the 3D position of the gold particle within the NPC channel is displayed in the graph using the gold-particle location coordinates (*y*, *l*). Fig. 4B also highlights the sampling bias of sectioning, whereby all sections through an NPC centre contain information about the periphery of the NPC, but not vice versa. As a consequence, a narrow range of sections represent the NPC centre compared with the periphery. This is because the NPC centre (radius 19 nm) is only sampled in sections through the NPC where the measured half width (*l*) is 38-42 nm, whereas sections of *l* ranging from 0 to 38 nm only sample the periphery (Fig. 4A). For this reason, in the graphs showing the raw data indicating the actual distributions of gold particles in the channel (the measured distance of the gold particle from the NPC section centre as a function of half the NPC section width, i.e. Fig. 4B, Fig. 5A, Fig. 6B), the grey NPC centre is relatively small compared with the white region representing the periphery.

We collected data sets on Kap104 cargo, Kap121 cargo, Gle1, Dbp5 and GFP positions within the NPC (Fig. 5A). The three graphs show that Kap104 and Kap121 cargos were primarily located close to the NPC edge (Fig. 5A, top; most of the data lie within the 'white' area of the graph, representing the peripheral NPC regions), whereas the locations of both Gle1 and Dbp5 were shifted towards the NPC centre (Fig. 5A, middle; gold particles accumulated towards the NPC centre, represented by the grey area of the graph). Finally, more uniform locations of the GFP are shown in the bottom graph in Fig. 5A (gold particles are equally distributed along the *y* axis – 'distance from the centre of the section, *y*').

The best fitting PDFs, which account for the sectioning bias, are shown in Fig. 5B. For the Kap104 cargo data, we found very strong evidence that the spatial distribution of particles was inconsistent with a uniform distribution (log-likelihood ratio test; G=15.6, df=2, P<0.001; null hypothesis for this test: 'the distribution of particles throughout the NPC is uniform'; for details of G and df, see Materials and Methods). Instead, the data suggest that, when Kap104 cargo is transported within the NPC, it is most likely to be located within 15-20 nm of the NPC edge (Fig. 5B, top, solid curve). Similarly, the Kap121 cargo data were also inconsistent with a uniform distribution (log-likelihood ratio test; G=50.38, df=2, P<0.001; null hypothesis for this test: 'the distribution of particles throughout the NPC is uniform'). Like Kap104, Kap121 cargo locations were estimated to lie mostly within 15 nm of the NPC edge (Fig. 5B top, dashed curve).

There is an inherent imprecision in the indirect immunogold labelling used here, due to the distance between the centre of the gold particle and the epitope, which could be between 0 and 15 nm, depending on how the antibodies are oriented in relation to the epitope (Murphy et al., 1988; Ban et al., 1994; Iborra and Cook, 1998). However, the resolution is sufficient to distinguish between

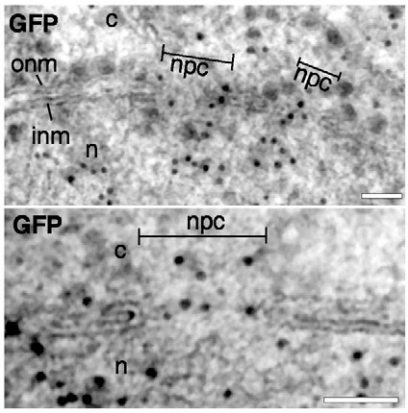

Fig. 3. Diffusion of GFP takes a random route via the NPC. Representative TEM micrographs of high-pressure frozen and freeze-substituted yeast expressing unconjugated GFP immunolabelled with polyclonal anti-GFP primary antibody and anti-rabbit secondary antibody conjugated to 5 nm gold. The position of gold particles reflects the random location of GFP when diffusing through the NPC. Scale bars: 50 nm.

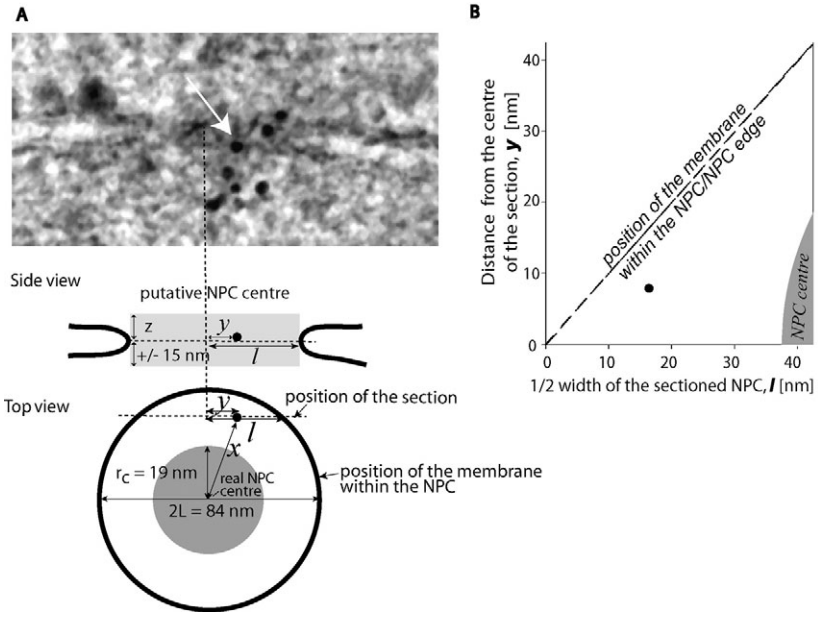

Fig. 4. Schematic of the NPC demonstrating the principles of measurement and plotting. (**A**) TEM micrograph showing an NPC section (top), a schematic of the NPC section, and the relationship between the section and the three-dimensional proportions of the NPC channel (bottom). Sections are cut randomly through the NPC and immunogold labelled for TEM imaging. The distance of the gold particle (the particle chosen for analysis is marked by the white arrow and further represented by a black circle) from the NPC centre (y) and the half width of the sectioned NPC (l) are measured to determine the actual distance of the gold particle from the NPC centre (x). The grey central circle shows the position of the 'central channel' or 'transporter' with a radius (r_c) of ~19 nm, as defined in Yang et al. (Yang et al., 1998) and Alber et al. (Alber et al., 2007). (**B**) Measured distances (l, y) are plotted for each data point to display the overall distribution of gold particles within the NPC. The dashed line marks the position of the NE and the grey area corresponds to the central area depicted in A. The black circle reflects the position of the gold particle in A.

central or edge distribution, even when the highest error is considered. Our best-fit models estimate that there is a 79% and 85% probability a Kap104 or Kap121 cargo label will be located within 15 nm of the edge of the channel, respectively, supporting our conclusion that these cargos are positively associated with the NPC edge. Furthermore, the PDF curve is very steep near the NPC edge, suggesting that it indeed reflects where the epitope is centred.

In addition, the Gle1 and Dbp5 locations within the NPC were both found to be inconsistent with a uniform distribution (Gle1: log-likelihood ratio test; G=32.0, df=2, P<0.001; Dbp5: log-likelihood ratio test; G=26.0, df=2, P<0.001; null hypothesis for both tests: 'the distribution of particles throughout the NPC is uniform'). However, they were both estimated to most likely be located within 20 nm of the NPC centre (Fig. 5B, middle; the probability of being located within the 20 nm of the NPC centre is 81% and 94% for Gle1 and Dbp5, respectively), suggesting that Gle1 and its Dbp5 binding partner were preferentially centrally located. Because the likelihood of cutting the section within the NPC centre (and thus spotting the central locations of the proteins) is much lower in comparison with the peripheral locations captured in every section, the centrally detected positions of Gle1 and Dbp5 confirm the reliability of our approach. Finally, the GFP locations were consistent with a uniform distribution (log-likelihood ratio test; G=0.26, df=2, P=0.88; Fig. 5B, bottom; null hypothesis for this test: 'the distribution of particles throughout the NPC is uniform'). Overall, these analyses show that the NPC central channel contains spatially distinguished areas for different routes of transport.

Loss of specific FG domains disabled Kap121- but not Kap104-dependent transport

As FG domains are currently thought to be highly important for the facilitated passage of cargo through the NPC, we investigated the role of specific FG domains in determining spatial aspects of nucleocytoplasmic transport. Mutant strains had already been constructed that possess the minimal combination of FG domains necessary to maintain viability (Strawn et al., 2004; Terry and Wente, 2007). Of those strains, we were particularly interested in the mutant *ΔNΔC Δnup100GLFG Δnup145GLFG* (*ΔN* and *ΔC* correspond to *nup1ΔFXFG nup2ΔFXFG nup Δ60FXF* and *nup159ΔFG nup42ΔFG*, respectively). Experiments with this set of FG deletions showed that there was a specific requirement for particular FG domains in the import of proteins dependent on either Kap104 or Kap121 (Terry and Wente, 2007). Whereas Kap121-dependent protein import was impaired in in situ nuclear import assays, Kap104-dependent import was still functional. We were interested in how the loss of FG domains spatially influenced both Kap121- and Kap104-dependent transport routes. We asked whether the transport of Kap121 and Kap104 cargos still occurred close to the edge, like it does in the wild type, or whether there were any modifications associated with the transport defect, for instance, the accumulation of the protein at the NPC entrance, which might explain the defect.

Interestingly, we found that the distribution of Kap104 cargo in the *ΔNΔC Δnup100GLFG Δnup145GLFG* mutant was consistent with the non-uniform spatial distribution of Kap104 we identified earlier for the wild type (log-likelihood ratio test; G=0.892, df=2, P=0.640; null hypothesis for this test: 'the distribution of gold particles between wild type and mutant is the same'). An example TEM micrograph is displayed in Fig. 6A. All data acquired for Kap104 cargo locations are presented in Fig. 6B, left. This graph clearly shows that, in the mutant, the majority of Kap104 cargo lies near the edge of the NPC. Fig. 6C, left, shows the best-fit PDFs for the wild type and the mutant, and illustrates their similarity, which is why our test was not statistically significant. This result suggests that active translocation of the Kap104 cargo near the channel periphery in the mutant is still functional, which is consistent with studies using biochemical assays (Terry and Wente, 2007).

By contrast, the spatial location of Kap121-dependent import differed between the mutant and the wild type (log-likelihood ratio test; G=30.2, df=2, P<0.001; null hypothesis for this test: 'the distribution of gold particles between wild type and mutant is the same'), and the data suggest that bias towards the NPC edge was lost in the mutant (Fig. 6B, right). In fact, the distribution of Kap121 cargos in the mutant strain was consistent with a uniform distribution (Fig. 6C, right, log-likelihood ratio test; G=0.76, df=2, P=0.684; null hypothesis for this test: 'the distribution of particles throughout the NPC is uniform'), which suggests that pathway

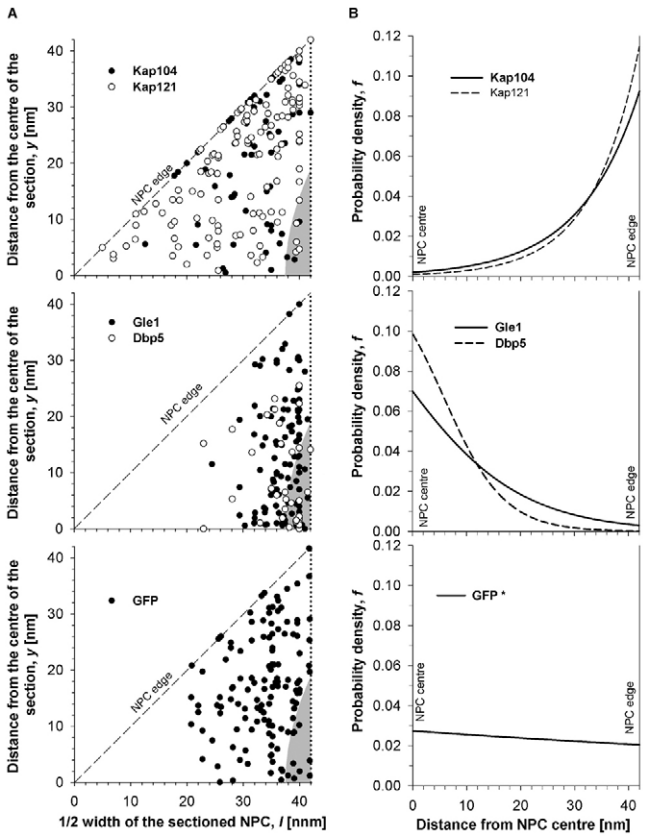

Fig. 5. Distribution of the various translocation markers within the NPC. (**A**) Positions of gold particles within the NPC in relation to the NPC width show the actual position of the particles within the NPC. Each circle represents a gold particle (reflecting the location of Kap104 and Kap121 cargos, Gle1, Dbp5 and GFP) within the NPC section. The dashed line delineates the position of the NPC edge and the grey area marks the NPC central area defined by radius 19 nm (Yang et al., 1998). (**B**) The best-fitting PDFs describing the position of cargos, Gle1, Dbp5 and GFP in relation to the horizontal distance (*x*) from the NPC centre. Whereas the best-fitting PDFs for both Kap121 and Kap104 cargos predicted an increasing likelihood of the Kap104 and Kap121 cargos being transported close to the NPC edge (top graph), the Gle1 and Dbp5 locations show the opposite trend (middle graph). The bottom graph shows the best fitting PDF for GFP. An asterisk indicates that this PDF is consistent with a uniform distribution. For Kap121 cargo *n*=130, for Kap104 cargo *n*=60, for Gle1 *n*=117, for Dbp5 *n*=33 and for GFP *n*=136.

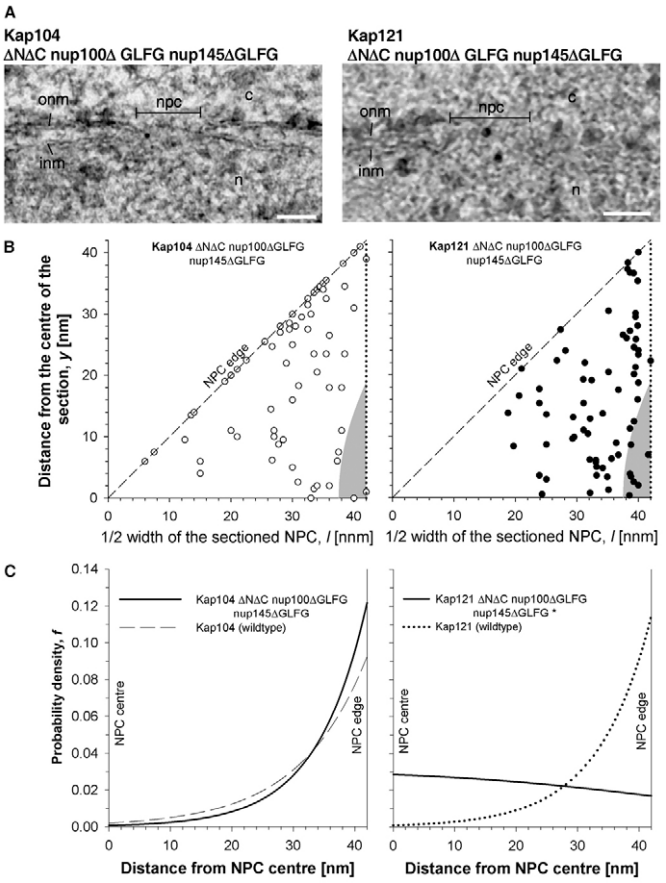

Fig. 6. In the *ΔNΔC nup100ΔGLFG nup145ΔGLFG* mutant, Kap121-dependent transport is affected. (**A**) Representative micrographs of Kap104 and Kap121 locations within the mutant NPC. (**B**) Graphs showing the positions of all analysed gold particles (reflecting the localisation of transported Kap104 and Kap121 cargos) in the mutant strain. The dashed line delineates the position of the NPC edge; the grey area marks the NPC central area. (**C**) The best-fitting models of Kap121 and Kap104 cargos within the NPC in the mutant strain (solid line) compared to the wild type. For wild-type data, see details in Fig. 3. An asterisk indicates that this PDF is consistent with a uniform distribution. For *ΔNΔC nup100ΔGLFG nup145ΔGLFG* mutant strain, Kap121 cargo *n*=77; Kap104 cargo *n*=76.

defects are present in the mutant. Our analysis supports earlier findings and provides direct insight into the spatial impact on NPC transport in an FG-domain mutant.

Discussion

We looked at the translocation process within individual NPCs in well preserved, cryofixed, immunogold-labelled yeast. To our knowledge, this is the first structural analysis that demonstrates the existence of spatially distinct transport routes through the NPC and the direct effect of FG-domain deletion on movement through the channel itself. Our findings are supported by previous evidence suggesting distinct biochemical routes for mRNA export and protein import (Strawn et al., 2001; Blevins et al., 2003; Terry and Wente, 2007). We found that protein import by Kap121 and Kap104, at least with the small cargos we have analysed, occurs preferentially at the NPC periphery. Importantly, our in vivo results are consistent with in vitro electron tomography experiments using isolated *Dictyostelium* nuclei, which showed that classical nuclear localization sequence (NLS)-cargo occupied the 20 nm central area of the channel with a relatively low density (Beck et al., 2007). This suggests that the peripheral transport route might be common to biochemically distinct import pathways and is conserved among organisms.

Our observation of the central location of mRNA export factors within the NPC channel is supported by previous observations of mRNA export showing that a very large mRNP complex, the Balbiani ring granule, was translocated centrally (Mehlin et al., 1995; Kiseleva et al., 1998). Moreover, Dbp5 was shown to travel through the NPC with the Balbiani ring granule mRNP complex in *Chironomus tentans* salivary glands (Zhao et al., 2002), suggesting

that it too could travel centrally. Previous studies of isolated nuclei or NEs have suggested that protein-A-tagged Dbp5 resides on the cytoplasmic fibrils of the NPC in yeast and vertebrates (Schmitt et al., 1999). The fibril localisation is consistent with our results because it has been shown that cytoplasmic filaments can extend into the centre of the NPC channel (Pante and Aebi, 1996; Rutherford et al., 1997; Goldberg et al., 2000). This conformation might not generally be well preserved during isolation of NEs and/or nuclei (Schmitt et al., 1999), but will be by high-pressure freezing. In fact, in gently isolated yeast nuclei, most NPC cytoplasmic filaments are indeed oriented towards the centre (J.F. and M.W.G., unpublished), which would locate fibril-bound molecules over the centre of the channel. As Dbp5 requires Gle1 for its activation, the overlap of Gle1 and Dbp5 locations within the NPC found here is consistent with their coordinated function in mRNA export (Alcazar-Roman et al., 2006; Bolger et al., 2008). The fact that Dbp5 and Gle1 have similar distributions in yeast NPCs strongly supports the hypothesis that mRNA export occurs through the centre of the channel.

Finally, our results suggested that the diffusion of GFP proceeds over the entire NPC width and thus overlaps with active translocation, as suggested previously (Feldherr and Akin, 1997; Keminer et al., 1999; Mohr et al., 2009). Importantly, this shows that the location of import to the periphery is not simply a default position due to occlusion of the centre by export complexes (Beck et al., 2007), but rather is a biochemically determined localization that is specific to facilitated import. Our data thus provide clues to the long-standing question of whether diffusion takes place separately from the active passage of cargo.

Our results are consistent with specific prior hypotheses and associated data regarding the NPC transport mechanism. In the proposed hydrogel-like scenario (Ribbeck and Gorlich, 2001; Frey and Gorlich, 2007), the permeability barrier is created by the sieve-like structure of interacting FG domains. Overcoming this barrier is achieved upon binding of the transport receptor and transient disorder of the meshwork. If applied to the hydrogel model, our results suggest that specific binding sites might have specific locations within the meshwork. Additionally, the meshwork might not be homogeneous, but rather structured and organized to allow segregation of binding sites for different Kaps and transport factors into different zones within the transport channel. Thus, binding sites for Kap121 and Kap104 might be located closer to the NPC periphery, whereas the terminal stages of mRNA export might be located more centrally, depending on the position of the necessary effectors, such as Gle1 or Dbp5 (Alcazar-Roman et al., 2006; Weirich et al., 2006; Tran et al., 2007). Simultaneously, diffusion of GFP, which does not rely on receptors, could proceed over the entire NPC width if the restrictive size of the sieves is larger than the diffusing object.

Models proposing random, undirected movement of cargo through the NPC based simply on virtual gating principles (Rout et al., 2000) and models assuming that the central part of the NPC channel is the only place for active translocation (Yang et al., 1998; Allen et al., 2000; Peters, 2005) are not supported by our findings. Our results also do not support models that restrict passive diffusion within distinct regions within the NPC (Hinshaw et al., 1992; Yang et al., 1998), but directly suggest that the process of passive diffusion can proceed unrestricted over the entire NPC width and thus overlap with facilitated translocation.

More complex models based on virtual gating are, however, consistent with our results. In the ‘brush-like’ model (Lim et al., 2006), the peripheral localization of the cargo after the reversible collapse of the FG domains upon cargo binding would be the expected consequence of translocation. Collapse of FG domains would result in their localization near the anchoring point, in other words near the NPC periphery. Larger cargos might require the coordinated assistance of more FG Nups positioned around the channel. This would result in more central translocation, as is seen in the case of 10 nm gold particles coated with nucleoplasmin and injected into *Xenopus* oocytes (Feldherr and Akin, 1997; Rutherford et al., 1997).

Significantly, a new model (the ‘Forest model’), based on in vitro biophysical studies of the properties and interactions of individual FG domains, predicts a highly organized structure of the NPC central channel containing different transport zones depending on the presence of specific FG domains (Yamada et al., 2010). This study, similar to our findings, suggested the existence of separate zones for the transport of cargos of larger and smaller sizes located at the inner or outer part of the NPC channel, respectively. According to this study, both zones would permit the diffusion of small molecules. Our results are in good agreement with these findings and thus provide direct in vivo evidence for the proposed model.

Our work also further analyzed the basis for the differential impact of the mutation *ΔNΔC Δnup100 GLFG Δnup145GLFG* on Kap121 versus Kap104 import (Terry and Wente, 2007). The peripheral localization, and coincident active transport, of Kap121 cargo was completely disabled by the deletions, resulting in Kap121 cargos moving through the NPC only by passive diffusion. This finding confirms that GLFG domains of Nup100 and Nup145 play indispensable roles in the facilitated passage of Kap121, but not Kap104, cargos. The results shown above demonstrate that our analysis is able to detect subtle changes and deviations in individual routes of passage through the NPC, and provide more detailed information on the process.

In conclusion, our immunoelectron microscopy approach, combined with statistical modelling, allowed us to distinguish between various spatial translocation routes. This is an important step necessary to understand the principles of nucleocytoplasmic transport and gating. Further analysis will be needed to reveal the spatial relationship between all the import and export pathways within the NPC, and the role of specific FG domains in their determination.

Materials and Methods

Plasmids and yeast strains

In this study, we used yeast strains SWY 2285 (genotype TRP1/trp1-1 LYS2/lys2 leu2-3,112/leu2-3,112 ura3-1/ura3-1 his3-11,15/his3-11,15) (Strawn et al., 2004) and SWY 3292 (genotype HA-LoxP-nup42ΔFG myc-LoxP-nup159ΔFG T7-LoxP-nup1ΔFXFGmyc-LoxP-nup2ΔFXFG myc-LoxP-nup60ΔFXF HA-LoxP-nup100ΔGLFG myc-LoxP-nup145ΔGLFG) (Terry and Wente, 2007). Yeast strains were grown in YPD (1% yeast extract, 2% peptone, 2% glucose) or in synthetic complete (SC) media with 2% glucose and lacking appropriate amino acids. Vectors used in this study are listed in supplementary material Table S1. Vector cloning was performed according to standard molecular biology strategies.

High-pressure freezing and freeze substitution of yeast for TEM

Cells in log phase were high-pressure frozen using a Leica EM PACT (Leica Microsystems, Wetzlar, Germany) according to the manufacturer’s instructions. Samples were then placed on top of frozen fixative (0.2% uranyl acetate, 0.2% glutaraldehyde, 0.01% osmium tetroxide, 5% H_2O in acetone), and cryofixed and dehydrated using the Leica EM AFS freeze-substitution unit programmed as follows. T1: –90°C 49 hours; S1: 5°C increment per hour up to –25°C; T2: –25°C 12 hours; S2 0°C 0 hours; T3: –25°C 50 hours. When the S2 step was finished, acetone washes were performed (2×15 minutes) and samples were infiltrated with Monostep Lowycril HM 20 at –25°C (Polysciences, Eppelheim, Germany) according to the manufacturer’s recommendations. The resin polymerisation was then initiated and

proceeded as follows. T1: –25°C 24 hours; S1: 5°C increment per hour up to 25°C; T2: 25°C 24-100 hours. When the polymerisation was finished, blocks were trimmed and 60 nm sections were cut for TEM immunogold labelling.

Immunogold labelling

Fresh sections were picked up on Formvar-coated nickel grids and rinsed with 0.1% glycine in PBS three times for 1 minute, blocked in 1% BSA in PBS four times for 1 minute and incubated with primary antibody in a wet chamber for 1 hour at room temperature. Excess antibody was removed by rinsing in PBS four times for 2 minutes. A secondary anti-rabbit antibody (Agar Scientific, Stansted, UK) conjugated with 5 nm colloidal gold diluted 1:20 was applied for 1 hour at room temperature. Grids were rinsed in PBS three times for 5 seconds, washed in PBS four times for 2 minutes and washed in distilled water ten times for 1 minute each before post-staining with 1% uranyl acetate for 10 minutes and Reynold's lead citrate for 10 minutes. Grids were air dried and observed at 120 kV accelerating voltage with a Hitachi H-7600 transmission electron microscope.

Primary antibodies used in this study were rabbit polyclonal anti-GFP (Abcam, Cambridge, UK) used in 1:50 dilution, affinity-purified rabbit polyclonal antibody against Gle1 (anti-Gle1) [WU851 (Suntharalingam et al., 2004)] in 1:10 dilution and affinity-purified rabbit polyclonal antibody against Dbp5 (anti-Dbp5) [ASW42 (Bolger et al., 2008)].

Data collection and analysis

To investigate the spatial organisation of transport routes within the NPC, we measured the positions of gold particles (reflecting the positions of Spo12-NLS-GFP, Nab2-NLS-GFP, GFP, Gle1 and Dbp5) within multiple NPCs on immunogold-labelled TEM sections. Based on the assumption that NPCs do not differ in size, we assumed that the radius of all NPCs (i.e. half the longest distance between the two membranes on TEM sections) was L=42 nm, as the longest measured distance between membranes was 84 nm. Previous estimates of this distance of the NPC have ranged between 78 and 84 nm (Yang et al., 1998; Alber et al., 2007). The actual horizontal distance from the cargo to the centre of the NPC, denoted x was determined using:

$$x(y,l) = \sqrt{L^2 - l^2 + y^2}\ , \tag{1}$$

where l is half the width of the sectioned NPC and y is the horizontal distance of the gold particle from the midway point of the sectioned NPC (see Fig. 4). For our analysis, we only selected images in which the cargo was within 15 nm of the NPC horizontal central plane (Fig. 4), as these are most likely to be in transit. All measurements were made using ImageJ software (http://rsbweb.nih.gov/ij/).

To describe how different transport pathways vary in relation to their distance from the NPC centre, we did the following. For each set of data associated with the distribution of Kap121, Kap104, Gle1, Dbp5 and GFP within the NPC, we sought a PDF, denoted $f(x)$, that best described the likelihood that a measured gold particle would be located at distance x from the centre of the NPC ($0 \le x \le L$). Unfortunately, $f(x)$ cannot be estimated directly from the distance measurements taken from sections, because sections do not always run through the centre of the NPC. However, assuming $f(x)$, and knowing the width of the sectioned NPC ($2l$), the likelihood that a gold particle will be located distance y from the centre of the NPC section is:

$$g(y,l) = c(l) f(x(y,l))\ , \tag{2}$$

where $c(l)$ is a normalising constant defined by:

$$c(l) = \left[\int_{z=0}^{l} f(x(z,l))\, dz \right]^{-1} . \tag{3}$$

Here, we assumed that $f(x)$ was logistic in form:

$$f(x) = \frac{c_0 \exp[b(x-a)]}{1 + \exp[b(x-a)]}\ , \tag{4}$$

where a and b are parameters and c_0 is the normalising constant,

$$c_0 = \left[\int_{z=0}^{L} \frac{\exp[b(z-a)]}{1 + \exp[b(z-a)]}\, dz \right]^{-1} . \tag{5}$$

The logistic function was chosen as it can describe three likely situations regarding the distribution of particles relative to the centre of the NPC. When b=0, $f(x)$ is constant, which is consistent with a random distribution of cargo particles. However, non-zero values of b reflect a monotonic increase (b>0) or a monotonic decrease (b<0) in cargo density with increasing distance from the centre of the NPC.

Models, defined by $f(x)$, were fitted to the data as follows. Suppose N NPCs were sectioned and analysed, and let the number of gold particles measured within NPC i be denoted n_i. Also, let l_i denote half the measured width of NPC i, and let $y_{i,j}$ denote the measured horizontal distance from the centre of the NPC to the j-th particle in the NPC ($1 \le j \le n_i$). The log-likelihood of the function $f(x)$, when defined by the parameters a and b, given the data (i.e. all the l_i and $y_{i,j}$), is

$$LL(a,b \mid \text{Data}) = \sum_{i=1}^{N} \sum_{j=1}^{n_i} \ln g(y_{i,j}, l_i)\ . \tag{6}$$

The best-fitting parameter estimates, also called maximum-likelihood parameter estimates, are the a and b that maximise Eqn 6.

Our analyses considered two types of statistical test. First, we looked for evidence that the distribution of particles throughout the NPC for the wild-type strains differed from a uniform distribution. Second, we looked for evidence that the distribution of particles differed between the mutant and the wild-type strains. For the first type of test, we considered two cases for $f(x)$. First, we assumed that cargo was randomly transported through the NPC by setting b=0, making $f(x)$=1/L. The maximum log-likelihood for this case (i.e. the value of Eqn 6) is denoted LL_0. Next, we examined the case in which both a and b were free to vary and found the maximum log-likelihood for the data (i.e. we found the a and b that maximise Eqn 6), which we denote LL_1. A log-likelihood ratio test was then used to see whether there was evidence that the non-uniform distribution better described the distribution of gold particles. The test statistic in this case is the deviance, defined by G=2(LL_1–LL_0). If the data were generated by the simpler model, then G is approximately chi-square distributed with two degrees of freedom (df), as the two models for $f(x)$ are nested and the more complex model has two additional free parameters (Sokal and Rohlf, 1994). For the second type of test, we combined the wild-type and the mutant data and fitted a single $f(x)$, allowing a and b to vary. Next, we fitted $f(x)$ separately to the wild-type and the mutant strain data, again allowing a and b to vary separately for each strain. For this test, LL_0 is the maximum log-likelihood when assuming a single $f(x)$ for both data sets and LL_1 is the sum of the two maximum log-likelihoods when assuming separate $f(x)$ for both data sets. The degrees of freedom for this test is also 2, as allowing the $f(x)$ to differ between the two strains requires two additional parameter estimates. In this case, rejecting the null hypothesis implies that there is evidence that the distribution of particles within the NPC differed between the wild-type and mutant strain. Results from all tests performed are summarized in supplementary material Table S2.

We thank Helen Grindley for technical support with immunogold labelling and image acquisition, and Christine Richardson for technical support. Also, we thank Laura Terry for advice on yeast handling. This work was supported by a grant from the Biotechnology and Biological Sciences Research Council, UK (grant number BB/E015735/1) to M.W.G. and a grant from the National Institutes of Health, USA (NIH R01 GM051219) to S.R.W. Deposited in PMC for release after 12 months.

Supplementary material available online at
http://jcs.biologists.org/cgi/content/full/123/16/2773/DC1

References

Akey, C. W. and Radermacher, M. (1993). Architecture of the Xenopus nuclear-pore complex revealed by 3-dimensional cryoelectron microscopy. *J. Cell Biol.* **122**, 1-19.

Alber, F., Dokudovskaya, S., Veenhoff, L. M., Zhang, W., Kipper, J., Devos, D., Suprapto, A., Karni-Schmidt, O., Williams, R., Chait, B. T. et al. (2007). The molecular architecture of the nuclear pore complex. *Nature* **450**, 695-701.

Alcazar-Roman, A. R., Tran, E. J., Guo, S. and Wente, S. R. (2006). Inositol hexakisphosphate and Gle1 activate the DEAD-box protein Dbp5 for nuclear mRNA export. *Nat. Cell Biol.* **8**, 711-716.

Allen, T. D., Cronshaw, J. M., Bagley, S., Kiseleva, E. and Goldberg, M. W. (2000). The nuclear pore complex: mediator of translocation between nucleus and cytoplasm. *J. Cell Sci.* **113**, 1651-1659.

Allen, N. P., Patel, S. S., Huang, L., Chalkley, R. J., Burlingame, A., Lutzmann, M., Hurt, E. C. and Rexach, M. (2002). Deciphering networks of protein interactions at the nuclear pore complex. *Mol. Cell Proteomics.* **1**, 930-946.

Ban, N., Escobar, C., Garcia, R., Hasel, K., Day, J., Greenwood, A. and McPherson, A. (1994). Crystal structure of an idiotype-anti-idiotype Fab complex. *Proc. Natl. Acad. Sci. USA* **91**, 1604-1608.

Bayliss, R., Littlewood, T. and Stewart, M. (2000). Structural basis for the interaction between FxFG nucleoporin repeats and importin-beta in nuclear trafficking. *Cell* **102**, 99-108.

Bayliss, R., Littlewood, T., Strawn, L. A., Wente, S. R. and Stewart, M. (2002). GLFG and FxFG nucleoporins bind to overlapping sites on importin-beta. *J. Biol. Chem.* **277**, 50597-50606.

Beck, M., Lucic, V., Forster, F., Baumeister, W. and Medalia, O. (2007). Snapshots of nuclear pore complexes in action captured by cryo-electron tomography. *Nature* **449**, 611-615.

Ben Efraim, I. and Gerace, L. (2001). Gradient of increasing affinity of importin beta for nucleoporins along the pathway of nuclear import. *J. Cell Biol.* **152**, 411-417.

Blevins, M. B., Smith, A. M., Phillips, E. M. and Powers, M. A. (2003). Complex formation among the RNA export proteins Nup98, Rae1/Gle2, and TAP. *J. Biol. Chem.* **278**, 20979-20988.

Bolger, T. A., Folkmann, A. W., Tran, E. J. and Wente, S. R. (2008). The mRNA export factor Gle1 and inositol hexakisphosphate regulate distinct stages of translation. *Cell* **134**, 624-633.

Chaves, S. R. and Blobel, G. (2001). Nuclear import of Spo12p, a protein essential for meiosis. *J. Biol. Chem.* **276**, 17712-17717.

Denning, D., Mykytka, B., Allen, N. P., Huang, L., Al, B. and Rexach, M. (2001). The nucleoporin Nup60p functions as a Gsp1p-GTP-sensitive tether for Nup2p at the nuclear pore complex. *J. Cell Biol.* **154**, 937-950.

Denning, D. P., Patel, S. S., Uversky, V., Fink, A. L. and Rexach, M. (2003). Disorder in the nuclear pore complex: the FG repeat regions of nucleoporins are natively unfolded. *Proc. Natl. Acad. Sci. USA* **100**, 2450-2455.

Devos, D., Dokudovskaya, S., Williams, R., Alber, F., Eswar, N., Chait, B. T., Rout, M. P. and Sali, A. (2006). Simple fold composition and modular architecture of the nuclear pore complex. *Proc. Natl. Acad. Sci. USA* **103**, 2172-2177.

Feldherr, C. M. and Akin, D. (1997). The location of the transport gate in the nuclear pore complex. *J. Cell Sci.* **110**, 3065-3070.

Frey, S. and Gorlich, D. (2007). A saturated FG-repeat hydrogel can reproduce the permeability properties of nuclear pore complexes. *Cell* **130**, 512-523.

Goldberg, M. W. and Allen, T. D. (1996). The nuclear pore complex and lamina: Three-dimensional structures and interactions determined by field emission in-lens scanning electron microscopy. *J. Mol. Biol.* **257**, 848-865.

Goldberg, M. W., Rutherford, S. A., Hughes, M., Cotter, L. A., Bagley, S., Kiseleva, E., Allen, T. D. and Clarke, P. R. (2000). Ran alters nuclear pore complex conformation. *J. Mol. Biol.* **300**, 519-529.

Hinshaw, J. E., Carragher, B. O. and Milligan, R. A. (1992). Architecture and design of the nuclear pore complex. *Cell* **69**, 1133-1141.

Hodge, C. A., Colot, H. V., Stafford, P. and Cole, C. N. (1999). Rat8p/Dbp5p is a shuttling transport factor that interacts with Rat7p/Nup159p and Gle1p and suppresses the mRNA export defect of xpo1-1 cells. *EMBO J.* **18**, 5778-5788.

Iborra, F. J. and Cook, P. R. (1998). The size of sites containing SR proteins in human nuclei. Problems associated with characterizing small structures by immunogold labeling. *J. Histochem. Cytochem.* **46**, 985-992.

Iglesias, N. and Stutz, F. (2008). Regulation of mRNP dynamics along the export pathway. *FEBS Lett.* **582**, 1987-1996.

Iovine, M. K. and Wente, S. R. (1997). A nuclear export signal in Kap95p is required for both recycling the import factor and interaction with the nucleoporin GLFG repeat regions of Nup116p and Nup100p. *J. Cell Biol.* **137**, 797-811.

Iovine, M. K., Watkins, J. L. and Wente, S. R. (1995). The GLFG repetitive region of the nucleoporin Nup116p interacts with Kap95p, an essential yeast nuclear import factor. *J. Cell Biol.* **131**, 1699-1713.

Keminer, O., Siebrasse, J. P., Zerf, K. and Peters, R. (1999). Optical recording of signal-mediated protein transport through single nuclear pore complexes. *Proc. Natl. Acad. Sci. USA* **96**, 11842-11847.

Kiseleva, E., Goldberg, M. W., Allen, T. D. and Akey, C. W. (1998). Active nuclear pore complexes in Chironomus: visualization of transporter configurations related to mRNP export. *J. Cell Sci.* **111**, 223-236.

Kramer, A., Liashkovich, I, Ludwig, Y. and Shahin, V. (2008). Atomic force microscopy visualises a hydrophobic meshwork in the central channel of the nuclear pore. *Pflugers Arch.* **456**, 155-162.

Lim, R. Y., Huang, N. P., Koser, J., Deng, J., Lau, K. H., Schwarz-Herion, K., Fahrenkrog, B. and Aebi, U. (2006). Flexible phenylalanine-glycine nucleoporins as entropic barriers to nucleocytoplasmic transport. *Proc. Natl. Acad. Sci. USA* **103**, 9512-9517.

Lim, R. Y., Fahrenkrog, B., Koser, J., Schwarz-Herion, K., Deng, J. and Aebi, U. (2007). Nanomechanical basis of selective gating by the nuclear pore complex. *Science* **318**, 640-643.

Lim, R. Y. H., Aebi, U. and Fahrenkrog, B. (2008). Towards reconciling structure and function in the nuclear pore complex. *Histochem. Cell Biol.* **129**, 105-116.

Macara, I. G. (2001). Transport into and out of the nucleus. *Microbiol. Mol. Biol. Rev.* **65**, 570-594.

Marelli, M., Aitchison, J. D. and Wozniak, R. W. (1998). Specific binding of the karyopherin Kap121p to a subunit of the nuclear pore complex containing Nup53p, Nup59p, and Nup170p. *J. Cell Biol.* **143**, 1813-1830.

Matsuura, Y., Lange, A., Harreman, M. T., Corbett, A. H. and Stewart, M. (2003). Structural basis for Nup2p function in cargo release and karyopherin recycling in nuclear import. *EMBO J.* **22**, 5358-5369.

Mehlin, H., Daneholt, B. and Skoglund, U. (1995). Structural interaction between the nuclear pore complex and a specific translocating RNP particle. *J. Cell Biol.* **129**, 1205-1216.

Mohr, D., Frey, S., Fischer, T., Guttler, T. and Gorlich, D. (2009). Characterisation of the passive permeability barrier of nuclear pore complexes. *EMBO J.* **28**, 2541-2553.

Murphy, R. M., Slayter, H., Schurtenberger, P., Chamberlin, R. A., Colton, C. K. and Yarmush, M. L. (1988). Size and structure of antigen-antibody complexes. Electron microscopy and light scattering studies. *Biophys. J.* **54**, 45-56.

Naim, B., Brumfeld, V., Kapon, R., Kiss, V., Nevo, R. and Reich, Z. (2007). Passive and facilitated transport in nuclear pore complexes is largely uncoupled. *J. Biol. Chem.* **282**, 3881-3888.

Pante, N. and Aebi, U. (1996). Sequential binding of import ligands to distinct nucleopore regions during their nuclear import. *Science* **273**, 1729-1732.

Patel, S. S., Belmont, B. J., Sante, J. M. and Rexach, M. F. (2007). Natively unfolded nucleoporins gate protein diffusion across the nuclear pore complex. *Cell* **129**, 83-96.

Peters, R. (2005). Translocation through the nuclear pore complex: selectivity and speed by reduction-of-dimensionality. *Traffic* **6**, 421-427.

Ribbeck, K. and Gorlich, D. (2001). Kinetic analysis of translocation through nuclear pore complexes. *EMBO J.* **20**, 1320-1330.

Rout, M. P., Aitchison, J. D., Suprapto, A., Hjertaas, K., Zhao, Y. M. and Chait, B. T. (2000). The yeast nuclear pore complex: composition, architecture, and transport mechanism. *J. Cell Biol.* **148**, 635-651.

Rutherford, S. A., Goldberg, M. W. and Allen, T. D. (1997). Three-dimensional visualization of the route of protein import: the role of nuclear pore complex substructures. *Exp. Cell Res.* **232**, 146-160.

Schmitt, C., von Kobbe, C., Bachi, A., Pante, N., Rodrigues, J. P., Boscheron, C., Rigaut, G., Wilm, M., Seraphin, B., Carmo-Fonseca, M. et al. (1999). Dbp5, a DEAD-box protein required for mRNA export, is recruited to the cytoplasmic fibrils of nuclear pore complex via a conserved interaction with CAN/Nup159p. *EMBO J.* **18**, 4332-4347.

Shulga, N., Mosammaparast, N., Wozniak, R. and Goldfarb, D. S. (2000). Yeast nucleoporins involved in passive nuclear envelope permeability. *J. Cell Biol.* **149**, 1027-1038.

Sokal, R. R. and Rohlf, F. J. (1994). *Biometry*. New York: W.H. Freeman and Company.

Solsbacher, J., Maurer, P., Vogel, F. and Schlenstedt, G. (2000). Nup2p, a yeast nucleoporin, functions in bidirectional transport of importin alpha. *Mol. Cell. Biol.* **20**, 8468-8479.

Stoffler, D., Feja, B., Fahrenkrog, B., Walz, J., Typke, D. and Aebi, U. (2003). Cryo-electron tomography provides novel insights into nuclear pore architecture: Implications for nucleocytoplasmic transport. *J. Mol. Biol.* **328**, 119-130.

Strawn, L. A., Shen, T. and Wente, S. R. (2001). The GLFG regions of Nup116p and Nup100p serve as binding sites for both Kap95p and Mex67p at the nuclear pore complex. *J. Biol. Chem.* **276**, 6445-6452.

Strawn, L. A., Shen, T., Shulga, N., Goldfarb, D. S. and Wente, S. R. (2004). Minimal nuclear pore complexes define FG repeat domains essential for transport. *Nat. Cell Biol.* **6**, 197-206.

Suntharalingam, M., Alcazar-Roman, A. R. and Wente, S. R. (2004). Nuclear export of the yeast mRNA-binding protein Nab2 is linked to a direct interaction with Gfd1 and to Gle1 function. *J. Biol. Chem.* **279**, 35384-35391.

Terry, L. J. and Wente, S. R. (2007). Nuclear mRNA export requires specific FG nucleoporins for translocation through the nuclear pore complex. *J. Cell Biol.* **178**, 1121-1132.

Tran, E. J., Zhou, Y., Corbett, A. H. and Wente, S. R. (2007). The DEAD-box protein Dbp5 controls mRNA export by triggering specific RNA: protein remodeling events. *Mol. Cell* **28**, 850-859.

Walther, P. and Ziegler, A. (2002). Freeze substitution of high-pressure frozen samples: the visibility of biological membranes is improved when the substitution medium contains water. *J. Microsc.* **208**, 3-10.

Weirich, C. S., Erzberger, J. P., Flick, J. S., Berger, J. M., Thorner, J. and Weis, K. (2006). Activation of the DExD/H-box protein Dbp5 by the nuclear-pore protein Gle1 and its coactivator InsP6 is required for mRNA export. *Nat. Cell Biol.* **8**, 668-676.

Yamada, J., Phillips, J. L., Patel, S., Goldfien, G., Calestagne-Morelli, A., Huang, H., Reza, R., Acheson, J., Krishnan, V. V., Newsam, S. et al. (2010). A bimodal distribution of two distinct categories of intrinsically-disordered structures with separate functions in FG nucleoporins. *Mol. Cell Proteomics* [Epub ahead of print] doi: 10.1074/mcp.M000035-MCP201

Yang, Q., Rout, M. P. and Akey, C. W. (1998). Three-dimensional architecture of the isolated yeast nuclear pore complex: functional and evolutionary implications. *Mol. Cell* **1**, 223-234.

Zhao, J., Jin, S. B., Bjorkroth, B., Wieslander, L. and Daneholt, B. (2002). The mRNA export factor Dbp5 is associated with Balbiani ring mRNP from gene to cytoplasm. *EMBO J.* **21**, 1177-1187.